Characterization of interactions between horseradish peroxidase and metallic nanoparticles – implications for detecting reactive oxygen species using 2',7'-dichlorofluorescin diacetate

Amanda Kessler,[a,*] Jonas Hedberg,[a] Sarah McCarrick,[b] Hanna Karlsson,[b] Eva Blomberg,[a, c] Inger Odnevall [a,*]

[a] KTH Royal Institute of Technology, Department of Chemistry, Div. Surface and Corrosion Science, Stockholm, Sweden

[b] Institute of Environmental Medicine, Karolinska Institutet, Stockholm, Sweden

[c] RISE Research Institutes of Sweden, Division Bioeconomy and Health, Material and Surface Design, Stockholm, Sweden

[*] Corresponding authors, email: akessler@kth.se or ingero@kth.se

Table S1. Summary of XPS results.

Binding energy (eV)	Peak	Assignment
Mn NPs		
641.3	Mn 2p3/2	Mn_3O_4/MnO_2/Mn_2O_3/MnOOH [1]
638.6	Mn 2p3/2	Mn(0) [2]
530.0	O 1s	Mn(II)/Mn(III)/Mn(IV) [2]
532.1	O 1s	Mn(II)/Mn(III)/Mn(IV) [2]
533.7	O 1s	Mn(II)/Mn(III)/Mn(IV) [2]
Ni NPs		
852.7	Ni 2p3/2	Ni(0) [2]
854.1	Ni 2p3/2	Ni_2O_3/NiOOH/ $Ni(OH)_2$ [2]
855.7	Ni 2p3/2	NiOOH/$Ni(OH)_2$/NiO [2]
858.0	Ni 2p3/2	NiOOH/ $Ni(OH)_2$ [2]
860.3	Ni 2p3/2	$Ni(OH)_2$ [2]
862.6	Ni 2p3/2	$Ni(OH)_2$ [2]
529.5	O 1s	Ni(II) [2]
531.6	O 1s	Ni(II) [2]
533.4	O 1s	Ni(II) [2]
Cu NPs		
933.1	Cu 2p3/2	Cu(0)/Cu_2O [3]
934.8	Cu 2p3/2	CuO/$Cu(OH)_2$ [1, 3]
940.7	Cu 2p3/2	CuO/$Cu(OH)_2$ [1, 3]
943.5	Cu 2p3/2	CuO/$Cu(OH)_2$ [1, 3]
529.8	O 1s	CuO [3]
531.7	O 1s	CuO/$Cu(OH)_2$ [3]

Infrared spectroscopy

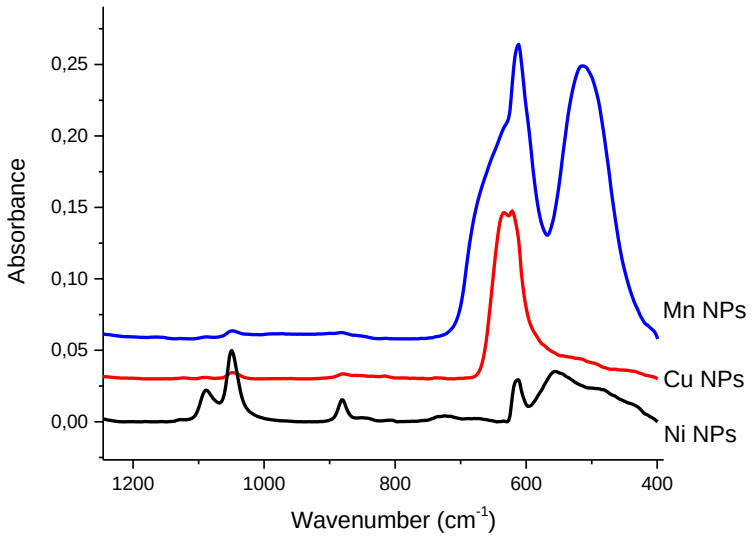

Figure S1. FTIR transmission spectroscopy on NP powder. The NPs were embedded in a KBr pellet**.**

Table S2. Summary and assignment of main vibrational bands in Figure S1.

Particle	**Peak position (cm^{-1})**	**Assignment**
Ni	487	$Ni(OH)_2$ [4, 5] ([6]
Ni	554	$Ni(OH)_2$ [4, 5, 7] ([6]
Ni	612	$Ni(OH)_2$ [6, 8]
Ni	879	
Ni	1049	CO_2/CO_3 [7]
Ni	1090	
Mn	611	Mn_3O_4[9, 10] [11, 12]
Mn	507	Mn_3O_4[9, 10] [11, 12]
Mn	403	Mn_3O_4[9, 10]
Mn	340	Mn_3O_4[9, 10]
Cu	635	Cu_2O [13]

Metal speciation calculations

Table S3. Metal ion concentrations used in the metal speciation calculations.

Solution	Concentration
Mn NaCl HRP	10 313 µg/L Mn^2
Mn NaCl	7763 µg/L Mn^{2+}
Mn PBS	1980 µg/L Mn^{2+}
Mn PBS+HRP	2377 Mn^{2+}
Mn DMEM	1500 µg/L Mn^{2+}
Ni NaCl + HRP	928 µg/L Ni^{2+}
Ni NaCl	1003 µg/L Ni^{2+}
Ni PBS	1177 µg/L Ni^{2+}
Ni PBS+HRP	1145 µg/L Ni^{2+}
Ni DMEM=	1500 µg/L Ni^{2+}
Cu NaCl+HRP=	1976 µg/L Cu^{2+}
Cu NaCl	938 µg/L Cu^{2+}
Cu PBS	420 µg/L Cu^{2+}
Cu PBS + HRP	442 µg/L Cu^{2+}
Cu DMEM	1500 µg/L Cu^{2+}

Table S4. Equilibrium calculations results for Mn ions in solution.

Mn, saline	Mn, saline, HRP	Mn, PBS	Mn, PBS, HRP
94.8% Mn^{2+}	94.8% Mn^{2+}	99.999% $MnHPO_4$(s)	99.999% $MnHPO_4$(s)
4.5% $MnCl^+$	4.5% $MnCl^+$	0.00074% $MnHPO_4$(aq)	0.00074% $MnHPO_4$(aq)
0.64% $MnCl_2^-$	0.64% $MnCl_2^-$	0.00024 Mn^{2+}	0.00024 Mn^{2+}

Table S5. Equilibrium calculations results for Cu ions in solution**.**

Cu, saline	Cu, saline, HRP	Cu, PBS	Cu, PBS, HRP
99.1% CuO(s)	99.6% CuO(s)	79.1% CuO(s)	80.2% CuO(s)
0.52% Cu^{2+}	0.23% Cu^{2+}	18.9% $CuHPO_4$(aq)	17.2% $CuHPO_§$(aq)
0.31% $CuOH^+$	0.14% $CuOH^+$	1.2% Cu^{2+}	1.1% Cu^{2+}
		0.83% $CuOH^+$	0.67% $CuOH^+$

Table S6. Equilibrium calculations results for Ni ions in solution. Tyr=Tyrosine, Cys=Cysteine, His=Histidine

Ni, saline	Ni, saline, HRP	Ni, PBS	Ni, PBS, HRP	Ni, DMEM
97.9% Ni^{2+}	97.9% Ni^{2+}	50.5% $NiHPO_4$(aq)	50.5% $NiHPO_4$(aq)	65%. $NiH_6Tyr_3^{2+}$
1.8% $NiCl^+$	1.8% $NiCl^+$	48.1% Ni^{2+}	48.1% Ni^{2+}	12%. $NiH_4Tyr_2^{2+}$
0.3% $NiOH^+$	0.3% $NiOH^+$	0.85% $NiCl^+$	0.85% $NiCl^+$	7%. $NiCys_2^{2-}$
				5%. $NiHisCys^-$
				5%. $NiHis_2$
				3% NiH_5Tyr^+
				1% $NiGlnCys^-$
				1% NiGlnHis

Table S7. Detection limit of AAS quantification for Mn, Ni, Cu. The detection limit was calculated from mean of 3 times the standard deviation of blank samples.

Sample series	Detection limit ug/L
Mn NaCl	0.5
Mn PBS	2.1
Ni NaCl	1.5
Ni PBS	6.1
Cu NaCl	3.2
Cu PBS	0.8

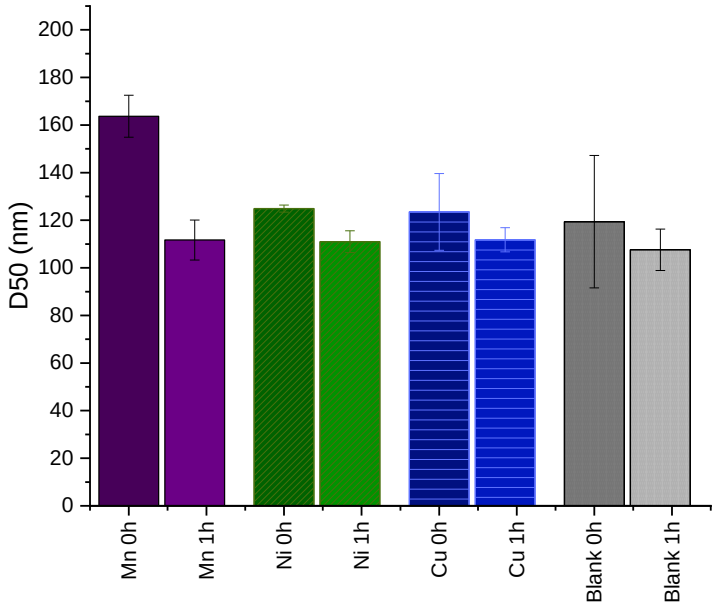

Figure S8. Particle size distributions determined by NTA for metal ions and PBS not significant particle size different with or without metal ions. HRP concentration was 8 u/mL. Metal ion concentrations added were the same as detected in metal release experiments with the same metal NPs.

References

1. Muilenberg, G.E. and C.D. Wagner, *Handbook of X-ray photoelectron spectroscopy : a reference book of standard data for use in X-ray photoelectron spectroscopy*. 1979, Eden Prairie, Minn.: Eden Prairie, Minn. : Perkin-Elmer.
2. Biesinger, M.C., et al., *Resolving surface chemical states in XPS analysis of first row transition metals, oxides and hydroxides: Cr, Mn, Fe, Co and Ni.* Applied Surface Science, 2011. **257**(7): p. 2717-2730.
3. Biesinger, M.C., *Advanced analysis of copper X-ray photoelectron spectra.* Surface and Interface Analysis, 2017. **49**(13): p. 1325-1334.
4. Rajamathi, M., P.V. Kamath, and R. Seshadri, *Polymorphism in nickel hydroxide: Role of interstratification.* Journal of Materials Chemistry, 2000. **10**(2): p. 503-506.
5. Krehula, S., et al., *Influence of Fe(III) doping on the crystal structure and properties of hydrothermally prepared β-Ni(OH)2 nanostructures.* Journal of Alloys and Compounds, 2018. **750**: p. 687-695.
6. Allahyar, S., et al., *Simple new synthesis of nickel oxide (NiO) in water using microwave irradiation.* Journal of Materials Science: Materials in Electronics, 2017. **28**(3): p. 2846-2851.

7. Aghazadeh, M., A.N. Golikand, and M. Ghaemi, *Synthesis, characterization, and electrochemical properties of ultrafine β-Ni(OH)2 nanoparticles.* International Journal of Hydrogen Energy, 2011. **36**(14): p. 8674-8679.
8. Ren, Y. and L. Gao, *From Three-Dimensional Flower-Like α-Ni(OH)2 Nanostructures to Hierarchical Porous NiO Nanoflowers: Microwave-Assisted Fabrication and Supercapacitor Properties.* Journal of the American Ceramic Society, 2010. **93**(11): p. 3560-3564.
9. Ashoka, S., G. Nagaraju, and G.T. Chandrappa, *Reduction of KMnO4 to Mn3O4 via hydrothermal process.* Materials Letters, 2010. **64**(22): p. 2538-2540.
10. Ishii, M., M. Nakahira, and T. Yamanaka, *Infrared absorption spectra and cation distributions in (Mn, Fe)3O4.* Solid State Communications, 1972. **11**(1): p. 209-212.
11. Li, Y., et al., *Synthesis of polyaniline nanotubes using Mn2O3 nanofibers as oxidant and their ammonia sensing properties.* Synthetic Metals, 2011. **161**(1): p. 56-61.
12. Ashoka, S., et al., *Synthesis and characterisation of microstructural α-Mn2O3 materials.* Journal of Experimental Nanoscience, 2010. **5**(4): p. 285-293.
13. Melendres, C.A., et al., *Synchrotron far infrared spectroscopy of surface films on a copper electrode in aqueous solutions.* Nuclear Inst. and Methods in Physics Research, B, 1997. **133**(1): p. 109-113.